

ARTICLE OPEN



Connection between the Tropical Pacific and Indian Ocean and Temperature Anomaly across West Antarctic

Ping Zhang ^{1,2} and Anmin Duan ^{1,2,3} ✉

West Antarctic and the Antarctic Peninsula have experienced dramatic warming in austral spring since the 1970s. Using observations and the Community Atmosphere Model version 4 (CAM4), this study explores the physical mechanism by which the tropical Pacific and Indian Ocean temperature anomaly mode (PIM) affects the dipolar surface air temperature (SAT) anomalies across the West Antarctic in austral spring. The positive phase of the PIM, characterized by positive sea surface temperature anomalies (SSTAs) in the tropical central-eastern Pacific and western Indian Ocean and negative SSTAs in the Maritime Continent, can generate two branches of stationary Rossby wave trains propagating from the tropical central Pacific and southeastern Indian Ocean to the West Antarctic, with an anticyclonic anomaly appearing over the Amundsen Sea. The northerlies advect warmer air to the Ross–Amundsen Seas, but southerlies advect colder air to the Antarctic Peninsula–Weddell Sea, resulting in the dipole of SAT anomalies over the West Antarctic. In this process, the role of tropical central-eastern Pacific SSTAs dominate, and it is amplified by the SSTAs around the Maritime Continent. The SSTAs in the western Indian Ocean combined with the SSTAs over the Maritime Continent further contribute to the western pole of the SAT. Only simulation that includes a prescribed PIM forcing can exactly reproduce the observations of the dipolar SAT response across the West Antarctic, indicating the need to treat the tropical Pacific and Indian Oceans as a unified whole.

npj Climate and Atmospheric Science (2023)6:49; <https://doi.org/10.1038/s41612-023-00381-8>

INTRODUCTION

A pronounced and dramatic warming in the West Antarctic and Antarctic Peninsula, more than twice as fast as the global average, has been reported^{1,2}. The strongest and most persistent warming occurred in austral spring [September–November (SON)]^{3,4}. This warming can further affect sea level rise⁵, ice-sheet loss⁶, sea ice retreat⁷, and shift in polar ecosystems⁸. In particular, the recent West Antarctic warming was modulated mainly by natural internal variability rather than anthropogenic forcing^{9,10}.

The idea of a tropics–Antarctic connection has long been established, particularly the impacts of tropical Pacific variability such as El Niño–Southern Oscillation (ENSO) or ENSO-like mode¹¹. The sea surface temperature anomaly (SSTA) in the tropical central or eastern Pacific triggers a southeastward-propagating Rossby wave train that interacts with the Amundsen Sea Low, thus resulting in anomalous Antarctic climate through wind-driven dynamic and thermodynamic responses^{12–22}. ENSO also affects the Antarctic climate by modulating the regional Ferrel Cell and associated meridional heat transport^{23–25}. In addition, in austral spring, ENSO strongly co-varies with the Indian Ocean Dipole (IOD) mode, which generates poleward Rossby wave trains to influence the climate anomalies in the high latitudes of the Southern Hemisphere^{26–29}. Indeed, the impacts of the IOD alone cannot extend to the Amundsen Sea and beyond when ENSO is absent^{30,31}.

ENSO and the IOD interact with each other by modulating the Walker circulation and the Indonesian throughflow^{32–34}. Therefore, the tropical Pacific and Indian Ocean, as a whole, are a tightly interconnected system^{35,36}. To demonstrate this cross-basin connection, the Pacific–Indian Ocean temperature anomaly mode (PIM) is proposed, which is an intrinsic mode of the tropical Indo-Pacific SSTAs with a tripole-like pattern. It is characterized by cold (warm)

SSTAs over the western Pacific–eastern Indian Ocean and warm (cold) SSTAs in the eastern Pacific and western Indian Ocean during the positive (negative) phase^{37,38}. Overall, the PIM resembles the combined ENSO–IOD system; it can be initiated either by ENSO or the IOD, with the former being the dominant driver and the latter having more sporadic effects^{38,39}. The PIM, however, has somewhat different climate effects from the combination of ENSO and IOD⁴⁰. In addition, the PIM captures the common ascending branch induced independently by both ENSO and IOD, located around the Maritime Continent. This local convective heating can also significantly affect the West Antarctic climate⁴¹.

However, to our knowledge, few studies have discussed the potential influence of the PIM on the Antarctic. Therefore, this work aims to examine the physical mechanisms by which the PIM affects the surface air temperature (SAT) across the West Antarctic in austral spring and further investigates the relative roles played by the different ocean basins of the PIM by conducting numerical simulations with an atmospheric general circulation model (AGCM).

RESULTS

Relationship between PIM and the West Antarctic SAT anomaly

Figure 1 shows the first empirical orthogonal function (EOF1) of SAT anomalies across the West Antarctic (Supplementary Fig. 1) in austral spring based on three different reanalysis datasets. All three show a similar spatial distribution, characterized by a dipole pattern with an inverse anomaly between the eastern Ross–Bellingshausen Sea (60°–90°S, 170°E–90°W) and Antarctic Peninsula–Weddell Sea (60°–90°S, 70°–10°W). The dipole pattern explains approximately 40%–50% of the total variance (Fig. 1a–c).

¹State Key Laboratory of Numerical Modeling for Atmospheric Sciences and Geophysical Fluid Dynamics (LASG), Institute of Atmospheric Physics, Chinese Academy of Sciences, Beijing, China. ²College of Earth Science, University of Chinese Academy of Sciences, Beijing, China. ³State Key Laboratory of Marine Environmental Science, College of Ocean and Earth Sciences, Xiamen University, Xiamen, China. ✉email: amduan@lasg.iap.ac.cn

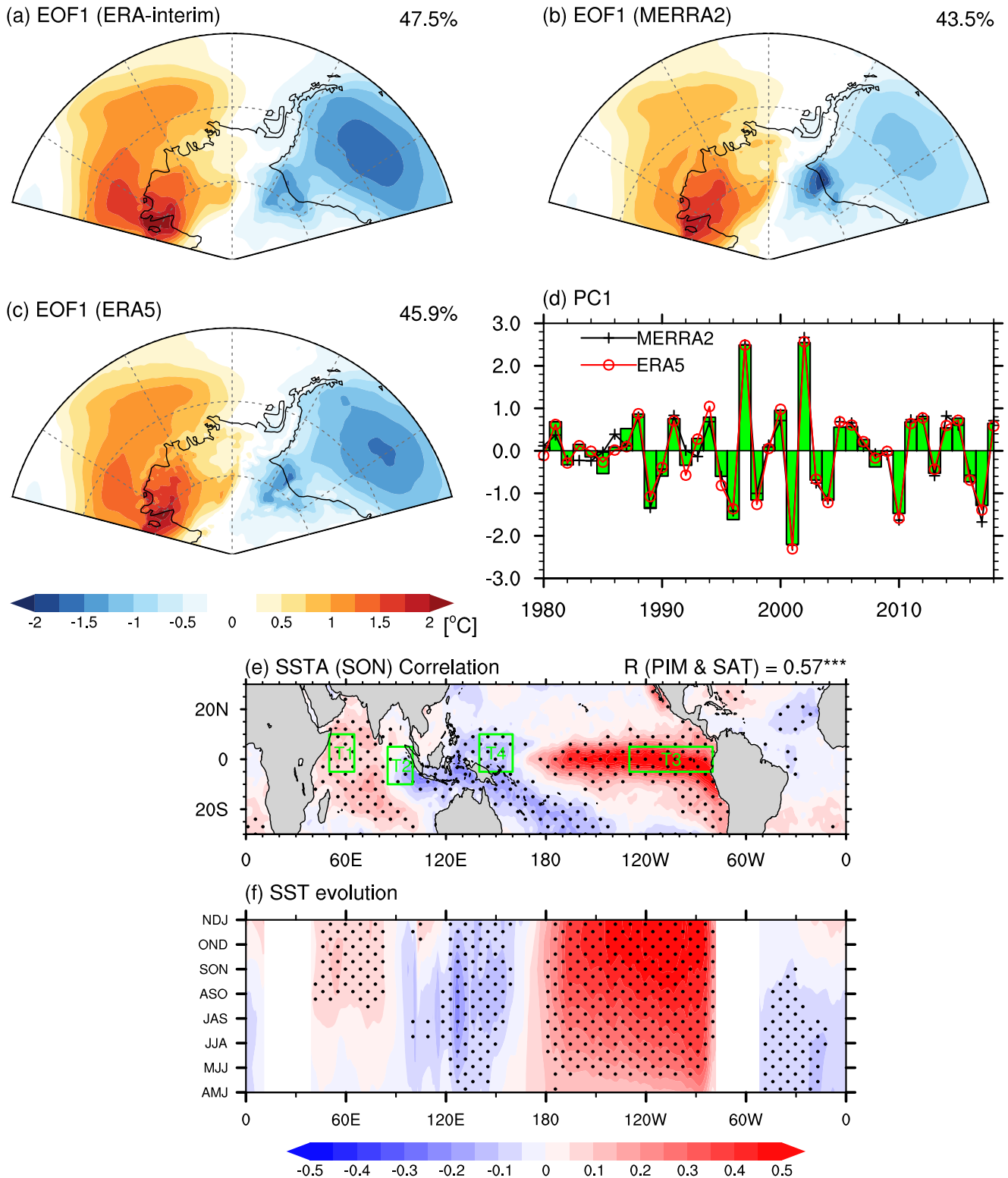


Fig. 1 West Antarctic Surface Air Temperature (SAT) anomaly in austral spring and its relationship with tropical SSTAs. Spatial patterns of the first empirical orthogonal function (EOF1) of the West Antarctic SAT (units: °C) derived from **a** ERA-Interim, **b** MERRA2, and **c** ERA5. Numbers in the upper-right corners indicate the percentage of variance explained by EOF1. **d** Normalized first principal component (PC1) of ERA-Interim (green bar), MERRA2 (black line), and ERA5 (red line); the PC1 of ERA-Interim is used to define the dipolar SAT index. **e** Simultaneous correlation between the tropical SSTAs and the SAT index in austral spring. The correlation coefficient between the Pacific and Indian Ocean temperature anomaly Mode (PIM) and the SAT indices is shown in the upper-right corner of **e**, and *** indicates the coefficient exceeding the 99% confidence level. The green box in **e** represents the key areas where the domain-averaged SSTA is used to define the PIM index. **f** Lead-lag correlation between the tropical SSTA averaged over 5°S–5°N from AMJ (April–May–June) to NDJ (November–December–January) and the SAT index in SON. Black stippling in **e**, **f** indicates regions with statistical significance above the 95% confidence level.

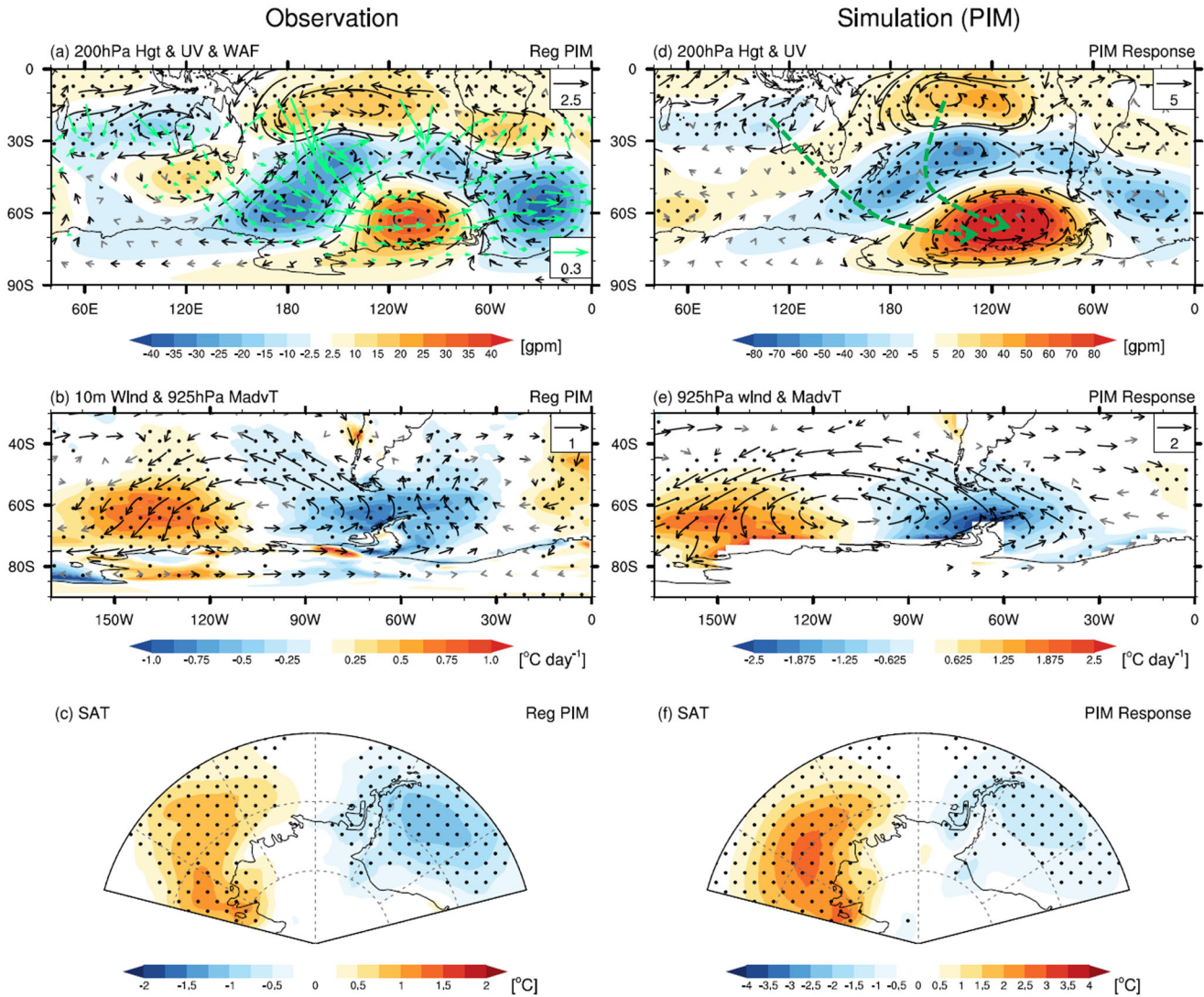


Fig. 2 Responses of the PIM in observations (left panel) and simulations (right panel). Observations (regression onto the PIM index): **a** 200-hPa geopotential height (shading; units: gpm), horizontal wind anomalies (black/gray vectors, units: m s^{-1}), and wave activity flux (WAF, green vectors; units: m s^{-1}); **b** 925-hPa meridional temperature advection $[-v(\partial T/\partial y)]$ (shading; units: $^{\circ}\text{C day}^{-1}$) and 10-m wind (vectors, m s^{-1}); **c** 2-m air temperature (units: $^{\circ}\text{C}$). Simulations (response of positive run minus negative run): **d–f** same as **a–c**, respectively, but for the responses in the PIM simulations. In **e**, 10-m wind is replaced by 925-hPa wind, because of the absence of 10-m wind output in the model. Black vectors and stippled regions indicate statistical significance above the 95% confidence level.

In addition, the first principal components (PC1) of the three datasets are also closely matched (Fig. 1d), indicating that the SAT variability is not dependent on the dataset. ERA-Interim is considered to be the most reliable reanalysis for depicting Southern Hemisphere high-latitudes climate^{42,43}. Therefore, the PC1 from ERA-Interim is utilized to define the dipole index of the West Antarctic SAT anomalies.

To explore the tropical SSTA drivers that can affect West Antarctic SAT, the simultaneous and lead–lag correlations of SSTAs with the spring SAT index are calculated (Fig. 1e–f). In austral spring, there is a tripolar pattern with positive–negative–positive SSTAs from west to east (Fig. 1e), which is characterized by warm SSTAs in the tropical central-eastern Pacific Ocean and the western Indian Ocean and cold SSTAs in the tropical southeastern Indian Ocean and western Pacific Ocean. The simultaneous correlation between the SAT and PIM indices reaches 0.57, significant at the 99% confidence level, and explains 32% of the variance of SAT. Due to the huge thermal inertia of seawater, a similar PIM-like pattern can be detected from July onward (Fig. 1f).

Therefore, it is reasonable to speculate that the PIM is a good precursor of the dipolar SAT anomaly over the West Antarctic.

Physical mechanism of the PIM affecting West Antarctic SAT

Figure 2 shows the responses to the PIM in the observations and simulations. In the observations (Fig. 2, left panel), corresponding to the positive phase of PIM, the 200-hPa geopotential height displays two branches of poleward-arching wave trains. The associated Takaya-Nakamura (T-N) flux shows that the wave energy originates from the tropical central-eastern Pacific and tropical southeastern Indian Ocean (Fig. 2a). The two wave trains feature an approximately equivalent barotropic structure in the extratropics and, conversely, a baroclinic structure over the tropical central-eastern Pacific and southeastern Indian Ocean (Supplementary Fig. 2). This is indicative of a classic stationary Rossby wave response to tropical SST forcing^{44,45}. That is, the PIM induces tripole-like convection anomalies by exciting an anomalous “double-loop” Walker circulation (Supplementary Fig. 3). Subsequently, the associated positive convective heating over the

tropical central-eastern Pacific and negative heating anomalies over the southeastern Indian Ocean can trigger a local upper-tropospheric anticyclonic and cyclonic anomalies, respectively, which act as Rossby wave sources, generating two branches of stationary Rossby wave trains propagating poleward. This causes an elongated anomalous high along with an anticyclonic anomaly over the Amundsen Sea (Fig. 2a). Onshore northerly anomalies to the west advect warmer air to the Ross–Amundsen Seas; in contrast, offshore southerly wind anomalies advect colder air to the Antarctic Peninsula–Weddell Sea (Fig. 2b). As a result, a dipole of SAT anomalies is formed in the West Antarctic (Fig. 2c).

Moreover, the responses in the PIM sensitivity experiment (Fig. 5) almost exactly reproduced the observations (Fig. 2, right panel), including the Pacific-induced and Indian Ocean-induced Rossby wave trains with the anomalous high over the Amundsen Sea (Fig. 2d), the dipolar meridional thermal advection (Fig. 2e), and the SAT dipole response across the West Antarctic (Fig. 2f). The close resemblance between the simulations and observations further verifies the above physical mechanism responsible for the PIM effect on the dipolar SAT anomaly over the West Antarctic in austral spring.

Relative role of different tropical ocean basins in driving West Antarctic SAT

To further examine the individual and combined effects of different tropical ocean basins of the PIM, another four sets of sensitivity runs are conducted (Model, Supplementary Table 1). Figure 3 shows the simulation results of the four sets of tropical ocean basin forcing. In the CEP run (Fig. 3a1, a2), the responses of circulation and SAT generally resemble those in the observations (Fig. 2a, c) and the PIM run (Fig. 2d, f). Warm SSTAs in the tropical central-eastern Pacific stimulate a southeastward stationary Rossby wave train, characterized by an anomalous high and anticyclone over the eastern Ross–Amundsen Seas (Fig. 3a1); this almost reproduces the dipole of SAT anomalies across the West Antarctic (Fig. 3a2), although its magnitude is much weaker than in the PIM simulation. That is, the tropical central-eastern Pacific SSTAs play a primary role in driving the dipolar SAT anomalies.

In the MC run (Fig. 3b1, b2), cold SSTAs around the Maritime Continent induce a weak wave train that stretches from the southeastern Indian Ocean to the western Ross Sea but cannot extend to the Amundsen Sea (Fig. 3b1). The Maritime Continent forcing alone fails to cause the dipolar SAT pattern in the West Antarctic (Fig. 3b2), but a Rossby wave train does appear to contribute to the anomalous high over the Amundsen Sea. Therefore, in the CEP and MC joint simulation (CEP + MC, Fig. 3c1, c2), the patterns of the responses closely resemble that forced by the PIM forcing. The two clear Rossby wave trains emanating from the central Pacific and southeastern Indian Ocean are well captured. They merge in the mid-latitudes of the southern Pacific, producing an anomalous high over the Amundsen Sea (Fig. 3c1), resulting in a stronger dipolar SAT response (Fig. 3c2) than in the CEP run. That is, the effect of the equatorial central-eastern Pacific SSTAs on the dipolar West Antarctic SAT is somewhat amplified by the SSTAs around the Maritime Continent. This is because the enhanced SST gradient in the tropical Pacific can excite an anomalous Walker circulation (Supplementary Fig. 3), which facilitates (suppresses) the anomalous convection over the equatorial central Pacific (southeastern Indian Ocean). Thus, the enhanced Rossby wave sources in these regions result in a stronger dipolar SAT response across the West Antarctic.

Note that the intensity and significance of the SAT response in the CEP + MC run (Fig. 3c2) are still weaker than those in the PIM run (Fig. 2f), especially for the western pole of the SAT response. Therefore, the WIO and MC joint simulation is conducted to further identify the potential contribution from the western Indian

Ocean. In the WIO + MC run (Fig. 3d1, d2), the enhanced zonal SST gradient between the western Indian Ocean and Maritime Continent restrains the suppressed convection over the Maritime Continent by inducing an anomalous Walker circulation in the tropical Indian Ocean (Supplementary Fig. 3), which further intensifies the Rossby wave source over the equatorial southeastern Indian Ocean. As a result, compared with the MC-alone run, the Rossby wave train response is more evident, although the anomalous high south of Australia shifts slightly westward. Including the western Indian Ocean SSTA results in an enhanced cyclonic anomaly in the western Ross Sea (Fig. 3d1). The warm advection east of the low-pressure center helps to warm the air mass over the Ross Sea (Fig. 3d2). That is, the SSTA dipole in the tropical Indian Ocean mainly influences the western pole of the SAT, which is consistent with the previous studies^{30,31}.

This study has explored the physical mechanism by which the PIM affects the dipolar SAT anomalies across the West Antarctic in austral spring, and further revealed the relative roles of the various ocean basins of the PIM using AGCM simulations. To summarize (Fig. 4), the tropical central-eastern Pacific dominates by exciting a poleward stationary Rossby wave train, while the Maritime Continent plays a subsidiary yet important role by amplifying the high-latitude response through triggering the Indian Ocean-induced wave train. The SSTAs in the western Indian Ocean combined with the SSTAs over the Maritime Continent contribute mainly to the western pole of the SAT by further suppressing the convection in the equatorial southeastern Indian Ocean. The above sensitivity experiments explicitly revealed the role of the various ocean basins, indicating the crucial importance of integrating the full system including both the tropical Pacific and Indian Oceans.

DISCUSSION

To complement the CAM4 simulation analyses, Rossby wave ray tracing, as a simplified theoretical Rossby wave model^{20,46,47}, was also employed to further investigate the dynamics of the PIM–West Antarctic teleconnection. The coherency among the observations, AGCM sensitivity experiments, and the Rossby wave ray tracing verify the robustness of the underlying mechanism for the PIM effect on the West Antarctic (Supplementary Fig. 4).

Note that the PIM has large persistence and develops from austral winter [June–August (JJA)] (Fig. 1f). The PIM–West Antarctic connection, however, can only be detected in SON. This may be resulted from both the local seasonality of background flow^{3,20,47–50} and the peak period of PIM^{38,39,51,52}. This study, therefore, is restricted solely to austral spring (SON).

Although the relative importance of different ocean basins has been identified in this work, their quantitative contributions remain unclear owing to nonlinear feedback. In future, model simulations with interannual variability will be conducted.

In addition to the PIM, there is also a robust correlation between the Southern Annular Mode (SAM) and the dipolar SAT anomalies, with a correlation coefficient of -0.57 (significant at the 99% confidence level). The PIM and SAM are independent of each other, with their correlation being only -0.13 . This motivates us to construct a multiple regression model using both the PIM and SAM indices to improve the simulation of the SAT anomalies. The reconstructed index explained nearly 57% of the West Antarctic SAT anomaly (Supplementary Table 2), and the SAT hindcast by the reconstructed index closely resembles the observations in terms of pattern and magnitude (Supplementary Fig. 5). The physical mechanism responsible for the effect of the SAM on the West Antarctic SAT and the combined effects induced by the PIM and SAM will be examined in another future work.

Tropical Atlantic SST forcing is known to be essential to drive climate variability over the West Antarctic. However, in SON, it is the PIM that dominates the interannual variability of West Antarctic climate, with a larger magnitude and significance of

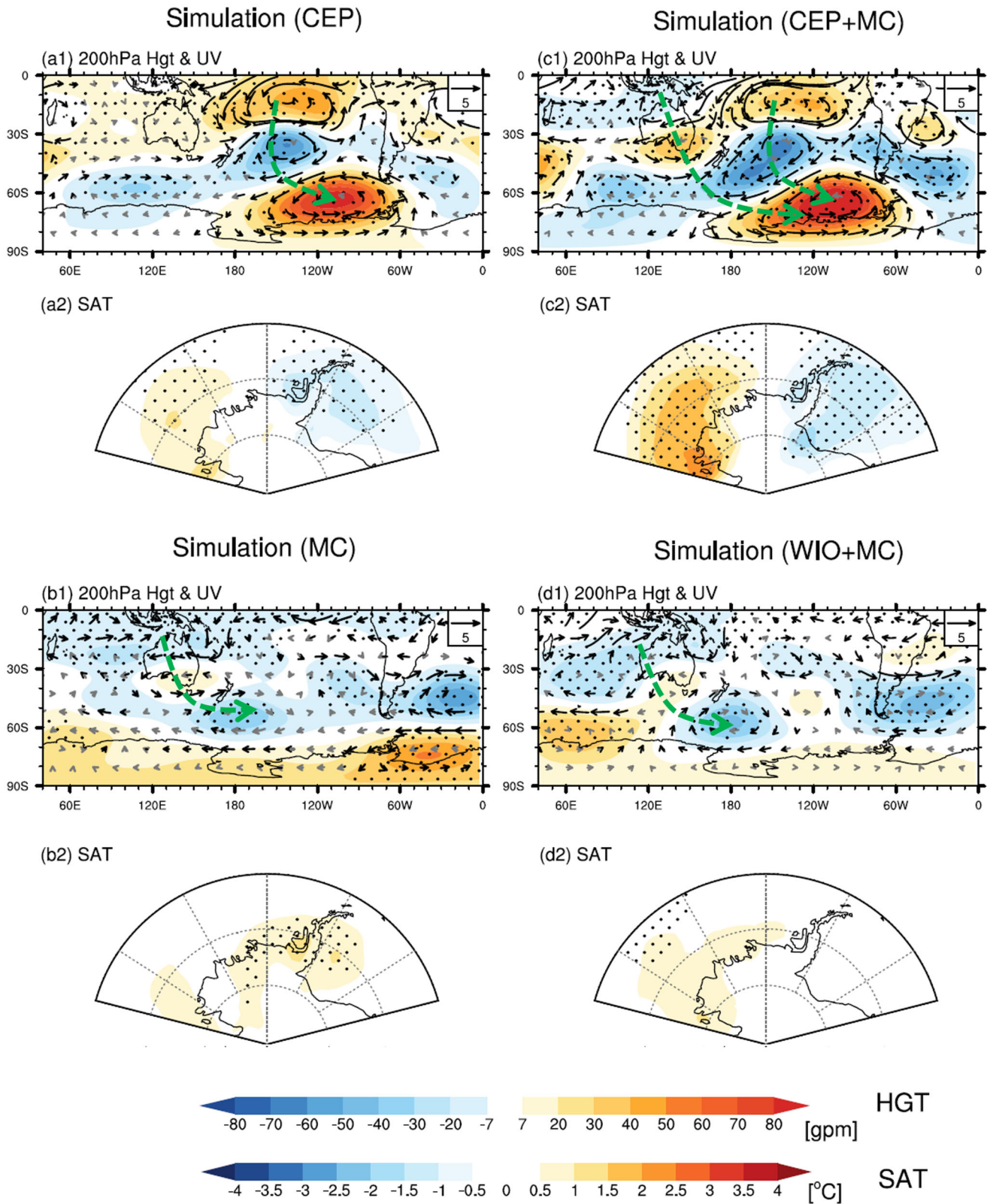


Fig. 3 Responses of circulation and SAT in four sets of sensitivity runs. CEP-alone run (top left panels): **a1** 200-hPa geopotential height (shading; units: gpm), horizontal wind anomalies (black/gray vectors, units: m s^{-1}); **a2** 2-m air temperature (units: $^{\circ}\text{C}$). **b1–b2**, **c1–c2**, and **d1–d2** Same as **a1–a2**, but for the responses in the MC-alone run (bottom left panels), CEP + MC run (top right panels), and WIO + MC run (bottom right panels), respectively. Black vectors and stippled regions indicate statistical significance above the 95% confidence level. Dashed green arrows represent the Rossby wave train.

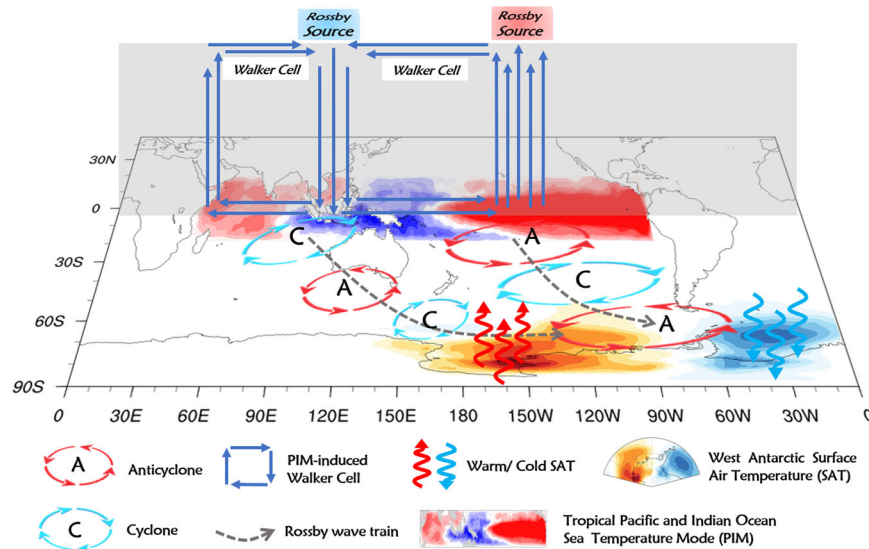


Fig. 4 Schematic diagram showing the physical mechanism by which the PIM affects the dipolar SAT anomaly across the West Antarctic in Austral Spring. The positive phase of the PIM excites an anomalous “double-loop” Walker circulation (blue vertical solid lines). The associated positive convective heating over the equatorial central-eastern Pacific and negative heating anomaly over the southeastern Indian Ocean act as Rossby wave sources (red/blue shading above gray board). They generate two branches of stationary Rossby wave trains propagating poleward (gray dash lines superimposed on alternating blue cyclones and red anticyclone), and thus induce an anticyclonic anomaly over the Amundsen Sea. The onshore northerly anomalies to the west advect warmer air to the Ross–Amundsen Seas (upward red wavy arrows, and orange shading). In contrast, the offshore southerly anomalies to the east cool the Antarctic Peninsula–Weddell Seas (downward blue wavy arrows, and blue shading). As a result, the dipolar SAT anomaly is formed across the West Antarctic. In this process, the tropical central-eastern Pacific SSTAs dominate, while the SSTAs over the Maritime Continent play a subsidiary yet important role by amplifying the high-latitude response by triggering a Rossby wave train. The SSTAs in the western Indian Ocean combined with the SSTAs over the Maritime Continent further contribute to the western pole of the SAT by inducing the anomalous Walker cell. Only simulation taking the tropical Pacific and Indian oceans as a unified whole can exactly match the observations of the dipolar SAT response across the West Antarctic.

SSTAs in the PIM regions (Fig. 1e). The interannual connection between the tropical Atlantic and Antarctic is restricted mainly to austral autumn⁵³ and winter^{47,54,55}. This can also be seen from the tropical SSTA evolution related to West Antarctic climate (Fig. 1f). In addition, the timescales of tropical SST variability differ significantly from one region to another. The tropical Atlantic becomes a dominant driver of West Antarctic climate on decadal timescales^{11,20,47,54,56,57}, and this is beyond the scope of this study.

METHODS

Data

The monthly mean datasets employed in this study are as follows: (1) SST data from HadISST1 at $1.0^\circ \times 1.0^\circ$ horizontal resolution⁵⁸, (2) atmospheric reanalysis data from the European Centre for Medium-range Weather Forecasts Interim reanalysis (ERA-Interim) at $1.5^\circ \times 1.5^\circ$ spatial resolution⁵⁹. The atmospheric variables used include 2-m temperature, wind, geopotential height, and sea level pressure. (3) Global Precipitation Climatology Project (GPCP) precipitation dataset at $2.5^\circ \times 2.5^\circ$ spatial resolution⁶⁰ is used to represent the deep convection activity. All datasets cover the period from 1980 to 2018.

The West Antarctic SAT index is defined as the first principal component (PC1) of the monthly SAT anomaly over the West Antarctic ($60^\circ\text{--}90^\circ\text{S}$, $170^\circ\text{E}\text{--}10^\circ\text{W}$) in austral spring. The PIM index is defined as $PIM = \nabla T_{\text{Indian}} + \nabla T_{\text{Pacific}}$ ($\nabla T_{\text{Indian}} = T1 - T2$, $\nabla T_{\text{Pacific}} = T3 - T4$), where $T1$, $T2$, $T3$, and $T4$ represent the domain-averaged SSTA in the regions ($50^\circ\text{E}\text{--}65^\circ\text{E}$, $5^\circ\text{S}\text{--}10^\circ\text{N}$), ($85^\circ\text{E}\text{--}100^\circ\text{E}$, $10^\circ\text{S}\text{--}5^\circ\text{N}$), ($130^\circ\text{W}\text{--}80^\circ\text{W}$, $5^\circ\text{S}\text{--}5^\circ\text{N}$), and ($140^\circ\text{E}\text{--}160^\circ\text{E}$, $5^\circ\text{S}\text{--}10^\circ\text{N}$), respectively, and the ∇T_{Indian} and $\nabla T_{\text{Pacific}}$ are normalized⁶¹. Before further analysis, all data have been Lanczos-filtered for 2–9 years after removing the linear trend

to focus on the interannual variability, which is the basis of any longer-term change.

Statistical analysis

Empirical Orthogonal Function (EOF) analysis is applied to detect the leading mode of West Antarctic SAT anomaly in austral spring. Takaya–Nakamura (T–N) wave activity flux⁶² is calculated to describe wave propagation generated by convective heating in the tropics. The T–N flux direction indicates the propagation of a large-scale Rossby wave. The two-tailed Student’s *t*-test is used to assess the statistical significance of the observations.

Model simulation

The atmospheric general circulation model (AGCM) employed here is CAM4.0 (Community Atmosphere Model version 4)⁶³, the atmospheric component of CESM1.2.0 (the Community Earth System Model, version 1.2.0)⁶⁴. The configuration of the horizontal resolution is 1.9° latitude \times 2.5° longitude (f19_g16) and the vertical resolution is 30 hybrid levels. The external forcing is fixed at the year-2000 level (F_2000). A control run and five sets of sensitivity runs are conducted (Fig. 5; Supplementary Table 1). The control run (CTRL) is forced by the climatological annual cycle of SST and integrated for 40 years. The first 8 years are used as spin-up and the last 32 years are used as the initial conditions to restart sensitivity runs. Each set of sensitivity runs consists of a positive and negative experiment and is integrated from May 1 to November 30. The prescribed SST forcing is the climatological SST augmented by different SSTA patterns in the tropical Pacific and Indian Ocean; for the positive (negative) runs, the SSTA patterns in the tropical Pacific and Indian Ocean are greater (less) than ± 1.0 standard deviation of the PIM index from July 1 to November 30 (the SSTA forcing in SON is shown in Fig. 5). A buffer zone (zonal and meridional ranges are

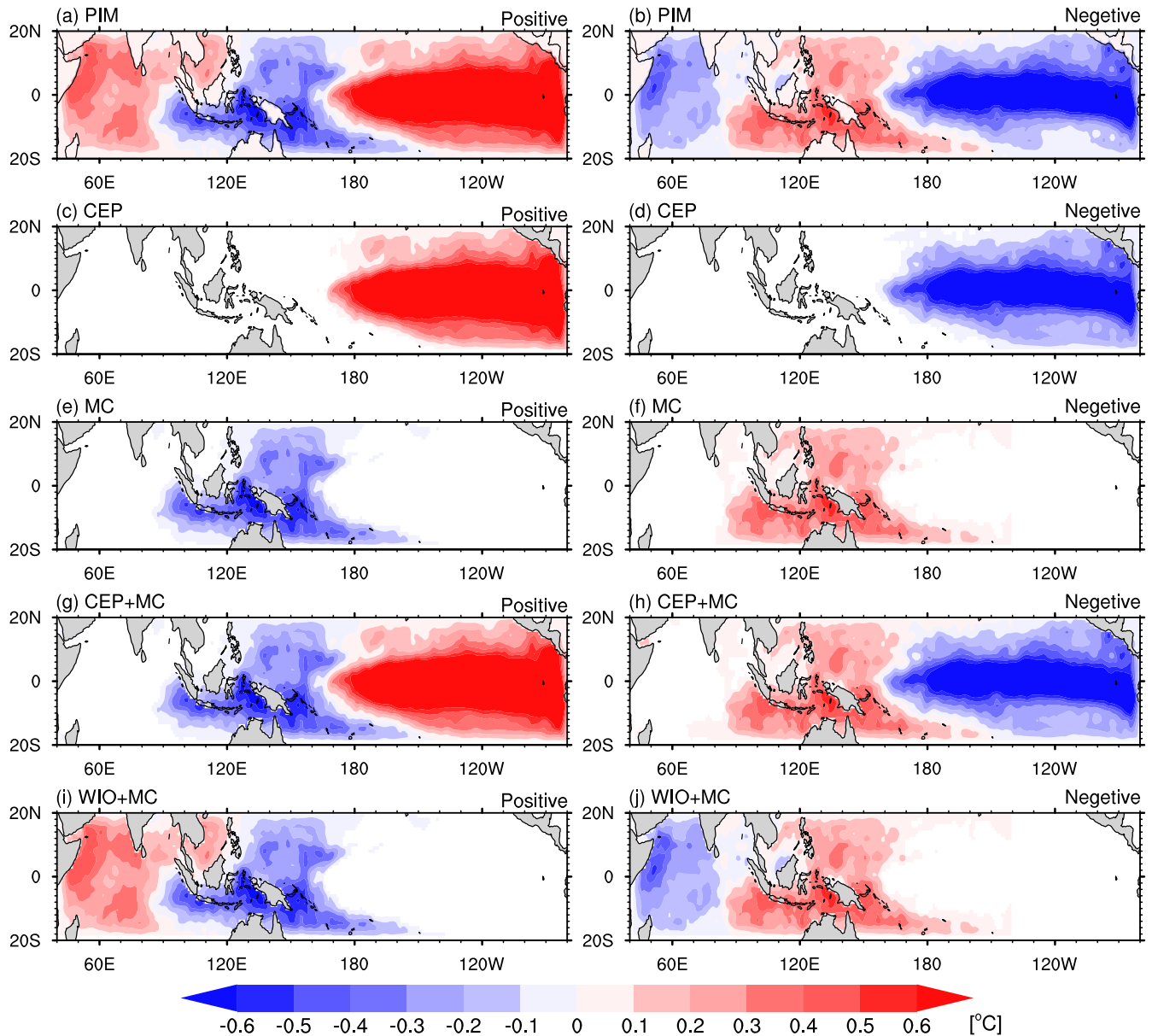


Fig. 5 SSTA forcing in austral spring of the five sets of sensitivity experiments. **a, b** SSTA forcing fields in the first set of sensitivity runs (PIM). **a** In the PIM positive run, the SSTA is prescribed in the tropical Pacific and Indian Ocean (20°S–20°N, 40°E–80°W), with the SSTA greater than +1.0 standard deviation of the PIM index; in contrast, in the PIM negative run **b**, the SSTA is less than –1.0 standard deviation of the PIM index. **c, d** As in **a, b**, but with only the SSTA forcing in the central-eastern Pacific (CEP) retained. **e, f** As in **a, b**, but with only the SSTA forcing in the Maritime Continent (MC) retained. **g, h** As in **a, b**, but with the combined SSTA forcing in the central-eastern Pacific and Maritime Continent retained (CEP + MC). **i, j** As in **a, b**, but with the combined SSTA forcing in the western Indian Ocean and Maritime Continent (WIO + MC) retained.

both 5°) is constructed between the forcing and other areas, with the restoration weight reduced linearly from one to zero. To remove the influence of atmospheric noise, each set of sensitivity experiments consists of 32 members, and the ensemble mean of the difference between positive and negative experiments is used to assess the robust responses for the specified SST forcing.

DATA AVAILABILITY

All the data are available. The ERA-Interim data is available online from <https://www.ecmwf.int/en/forecasts/datasets/reanalysis-datasets/era-interim>. Dataset of GPCP precipitation is from <https://psl.noaa.gov/data/gridded/data.gpcp.html>. HadISST1 is from <https://www.metoffice.gov.uk/hadobs/hadisst/data/download.html>. Output from the CESM experiments is available from the authors upon request.

CODE AVAILABILITY

All the codes used here are available from the corresponding author upon reasonable request.

Received: 8 November 2022; Accepted: 16 May 2023;
Published online: 27 May 2023

REFERENCES

- Steig, E. J. et al. Warming of the Antarctic ice-sheet surface since the 1957 International Geophysical Year. *Nature* **457**, 459–462 (2009).
- Clem, K. R. et al. Record warming at the South Pole during the past three decades. *Nat. Clim. Change* **10**, 762–770 (2020).

3. Schneider, D. P., Deser, C. & Okumura, Y. An assessment and interpretation of the observed warming of West Antarctica in the austral spring. *Clim. Dyn.* **38**, 323–347 (2011).
4. Nicolas, J. P. & Bromwich, D. H. New reconstruction of antarctic near-surface temperatures: multidecadal trends and reliability of global reanalyses. *J. Clim.* **27**, 8070–8093 (2014).
5. DeConto, R. M. & Pollard, D. Contribution of Antarctica to past and future sea-level rise. *Nature* **531**, 591–597 (2016).
6. Steig, E. J. How fast will the Antarctic ice sheet retreat? *Science* **364**, 936–937 (2019).
7. Stammerjohn, S., Massom, R., Rind, D. & Martinson, D. Regions of rapid sea ice change: an inter-hemispheric seasonal comparison. *Geophys. Res. Lett.* **39**, L06501 (2012).
8. Sahade, R. et al. Climate change and glacier retreat drive shifts in an Antarctic benthic ecosystem. *Sci. Adv.* **1**, e1500050 (2015).
9. Jones, J. M. et al. Assessing recent trends in high-latitude Southern Hemisphere surface climate. *Nat. Clim. Change* **6**, 917–926 (2016).
10. Turner, J. et al. Absence of 21st-century warming on Antarctic Peninsula consistent with natural variability. *Nature* **535**, 411–415 (2016).
11. Li, X. et al. Tropical teleconnection impacts on Antarctic climate changes. *Nat. Rev. Earth Environ.* **2**, 680–698 (2021).
12. Turner, J. The El Niño-southern oscillation and Antarctica. *Int. J. Climatol.* **24**, 1–31 (2004).
13. Lachlan-Cope, T. & Connolley, W. Teleconnections between the tropical Pacific and the Amundsen-Bellinghousens Sea: role of the El Niño/Southern Oscillation. *J. Geophys. Res.* **111**, D23101 (2006).
14. Ding, Q., Steig, E. J., Battisti, D. S. & Küttel, M. Winter warming in West Antarctica caused by central tropical Pacific warming. *Nat. Geosci.* **4**, 398–403 (2011).
15. Ding, Q., Steig, E. J., Battisti, D. S. & Wallace, J. M. Influence of the tropics on the southern annular mode. *J. Clim.* **25**, 6330–6348 (2012).
16. Ding, Q. & Steig, E. J. Temperature change on the antarctic Peninsula linked to the tropical pacific. *J. Clim.* **26**, 7570–7585 (2013).
17. Clem, K. R., Renwick, J. A. & McGregor, J. Large-scale forcing of the amundsen sea low and its influence on sea ice and west antarctic temperature. *J. Clim.* **30**, 8405–8424 (2017).
18. Clem, K. R. & Fogt, R. L. South Pacific circulation changes and their connection to the tropics and regional Antarctic warming in austral spring, 1979–2012. *J. Geophys. Res.* **120**, 2773–2792 (2015).
19. Yuan, X., Kaplan, M. R. & Cane, M. A. The interconnected global climate system—a review of tropical–polar teleconnections. *J. Clim.* **31**, 5765–5792 (2018).
20. Li, X., Holland, D. M., Gerber, E. P. & Yoo, C. Rossby waves mediate impacts of tropical oceans on west antarctic atmospheric circulation in austral winter. *J. Clim.* **28**, 8151–8164 (2015b).
21. Xin, M. et al. Characteristic features of the antarctic surface air temperature with different reanalyses and in situ observations and their uncertainties. *Atmosphere* **14**, 464 (2023).
22. Zhang, C., Li, T. & Li, S. Impacts of CP- and EP-El Niño events on the Antarctic sea ice in austral spring. *J. Clim.* **34**, 9327–9348 (2021).
23. Liu, J., Yuan, X., Rind, D. & Martinson, D. G. Mechanism study of the ENSO and southern high latitude climate teleconnections. *Geophys. Res. Lett.* **29**, 24-1-24-4 (2002).
24. Yuan, X. ENSO-related impacts on Antarctic sea ice: a synthesis of phenomenon and mechanisms. *Antarct. Sci.* **16**, 415–425 (2004).
25. Li, Y. et al. Interannual variability of regional hadley circulation and El Niño interaction. *Geophys. Res. Lett.* **50**, e2022GL102016 (2023).
26. Cai, W., van Rensch, P., Cowan, T. & Hendon, H. H. Teleconnection pathways of ENSO and the IOD and the mechanisms for impacts on Australian rainfall. *J. Clim.* **24**, 3910–3923 (2011).
27. Meehl, G. A. et al. Sustained ocean changes contributed to sudden Antarctic sea ice retreat in late 2016. *Nat. Commun.* **10**, 14 (2019).
28. Purich, A. & England, M. H. Tropical teleconnections to Antarctic Sea Ice during Austral spring 2016 in coupled pacemaker experiments. *Geophys. Res. Lett.* **46**, 6848–6858 (2019).
29. Wang, G. et al. Compounding tropical and stratospheric forcing of the record low Antarctic sea-ice in 2016. *Nat. Commun.* **10**, 13 (2019).
30. Nuncio, M. & Yuan, X. The influence of the Indian ocean dipole on antarctic sea ice. *J. Clim.* **28**, 2682–2690 (2015).
31. Feng, J., Zhang, Y., Cheng, Q., Liang, X. S. & Jiang, T. Analysis of summer Antarctic sea ice anomalies associated with the spring Indian Ocean dipole. *Glob. Planet. Change* **181**, 102982 (2019).
32. Yuan, D., Zhou, H. & Zhao, X. Interannual climate variability over the tropical pacific ocean induced by the indian ocean dipole through the Indonesian throughflow. *J. Clim.* **26**, 2845–2861 (2013).
33. Li, X. et al. Local and remote SST variability contribute to the westward shift of the Pacific Walker circulation during 1979–2015. *Geosci. Lett.* **8**, 1–11 (2021).
34. Cai, W. J. et al. Pantropical climate interactions. *Science* **363**, eaav4236 (2019).
35. Meehl, G. A., Arblaster, J. M. & Loschnigg, J. Coupled ocean-atmosphere dynamical processes in the tropical Indian and Pacific Oceans and the TBO. *J. Clim.* **16**, 2138–2158 (2003).
36. Wang, C. Three-ocean interactions and climate variability: a review and perspective. *Clim. Dyn.* **53**, 5119–5136 (2019).
37. Li, C. Y., Li, X., Yang, H., Pan, J. & Li, G. Tropical Pacific–Indian Ocean associated mode and its climatic impacts. *Chin. J. Atmos. Sci. (Chin.)* **42**, 505–523 (2018).
38. Chen, D. K. Indo-Pacific tripole: an intrinsic mode of tropical climate variability. *Adv. Geosci.* **24**, 1–18 (2011).
39. Lian, T., Chen, D., Tang, Y. & Jin, B. A theoretical investigation of the tropical Indo-Pacific tripole mode. *Sci. China Earth Sci.* **57**, 174–188 (2013).
40. Zhang, P. & Duan, A. Dipole mode of the precipitation anomaly over the tibetan plateau in mid-autumn associated with tropical pacific-indian ocean sea surface temperature anomaly: role of convection over the northern maritime continent. *J. Geophys. Res.* **126**, e2021JD034675 (2021).
41. Chen, J., Hu, X., Yang, S., Lin, S. & Li, Z. Influence of convective heating over the maritime continent on the West Antarctic Climate. *Geophys. Res. Lett.* **49**, e2021GL097322 (2022).
42. Bracegirdle, T. J. & Marshall, G. J. The reliability of antarctic tropospheric pressure and temperature in the latest global reanalyses. *J. Clim.* **25**, 7138–7146 (2012).
43. Jones, R. W. et al. Evaluation of four global reanalysis products using in situ observations in the Amundsen Sea Embayment, Antarctica. *J. Geophys. Res.* **121**, 6240–6257 (2016).
44. Gill, A. E. Some simple solutions for heat-induced tropical circulation. *Q. J. R. Meteorol. Soc.* **106**, 447–462 (1980).
45. Mo, K. C. & Higgins, R. W. The Pacific-South American modes and tropical convection during the Southern Hemisphere winter. *Monthly Weather Rev.* **126**, 1581–1596 (1998).
46. Hoskins, B. J. & Karoly, D. J. The steady linear response of a spherical atmosphere to thermal and orographic forcing. *J. Atmos. Sci.* **38**, 1175–1196 (1981).
47. Li, X., Gerber, E. P., Holland, D. M. & Yoo, C. A Rossby wave bridge from the tropical Atlantic to West Antarctica. *J. Clim.* **28**, 2256–2273 (2015a).
48. Jin, D. & Kirtman, B. P. Why the Southern Hemisphere ENSO responses lead ENSO. *J. Geophys. Res.* **114**, D23101 (2009).
49. Jin, D. & Kirtman, B. P. How the annual cycle affects the extratropical response to ENSO. *J. Geophys. Res.* **115**, D06102 (2010).
50. Scott Yiu, Y. Y. & Maycock, A. C. On the seasonality of the El Niño teleconnection to the Amundsen Sea Region. *J. Clim.* **32**, 4829–4845 (2019).
51. Li, X. & Li, C. The tropical Pacific–Indian Ocean associated mode simulated by LICOM2.0. *Adv. Atmos. Sci.* **34**, 1426–1436 (2017).
52. Yang, M., Li, X., Shi, W., Zhang, C. & Zhang, J. The Pacific-Indian Ocean associated mode in CMIP5 models. *Ocean Sci.* **16**, 469–482 (2020).
53. Ren, X. et al. Influence of tropical Atlantic meridional dipole of sea surface temperature anomalies on Antarctic autumn sea ice. *Environ. Res. Lett.* **17**, 094046 (2022).
54. Li, X., Holland, D. M., Gerber, E. P. & Yoo, C. Impacts of the north and tropical Atlantic Ocean on the Antarctic Peninsula and sea ice. *Nature* **505**, 538–542 (2014).
55. Simpkins, G. R., Peings, Y. & Magnusdottir, G. Pacific influences on tropical Atlantic teleconnections to the Southern Hemisphere high latitudes. *J. Clim.* **29**, 6425–6444 (2016).
56. Simpkins, G. R., McGregor, S., Taschetto, A. S., Ciasto, L. M. & England, M. H. Tropical connections to climatic change in the extratropical southern hemisphere: the role of Atlantic SST Trends. *J. Clim.* **27**, 4923–4936 (2014).
57. Okumura, Y. M., Schneider, D., Deser, C. & Wilson, R. Decadal–interdecadal climate variability over Antarctica and linkages to the tropics: analysis of ice core, instrumental, and tropical proxy data. *J. Clim.* **25**, 7421–7441 (2012).
58. Rayner, N. A. et al. Global analyses of sea surface temperature, sea ice, and night marine air temperature since the late nineteenth century. *J. Geophys. Res.* **108**, 4407 (2003).
59. Dee, D. P. et al. The ERA-Interim reanalysis: configuration and performance of the data assimilation system. *Q. J. R. Meteorol. Soc.* **137**, 553–597 (2011).
60. Huffman, G. J. et al. Global precipitation at one-degree daily resolution from multisatellite observations. *J. Hydrometeorol.* **2**, 36–50 (2001).
61. Yang, H., Jia, X. & Li, C. The tropical Pacific–Indian Ocean temperature anomaly mode and its effect. *Chin. Sci. Bull.* **51**, 2878–2884 (2006).
62. Takaya, K. & Nakamura, H. A formulation of a phase-independent wave-activity flux for stationary and migratory quasigeostrophic eddies on a zonally varying basic flow. *J. Atmos. Sci.* **58**, 608–627 (2001).
63. Gent, P. R. et al. The community climate system model version 4. *J. Clim.* **24**, 4973–4991 (2011).
64. Hurrell, J. W. et al. The community earth system model: a framework for collaborative research. *Bull. Am. Meteor. Soc.* **94**, 1339–1360 (2013).

ACKNOWLEDGEMENTS

This work was jointly supported by the National Natural Science Foundation of China (Grant Nos. 42030602, 41725018, and 91937302).

AUTHOR CONTRIBUTIONS

P.Z. carried out the data analysis, conducted the numerical experiments, and wrote the original manuscript. A.D. offered proposals, revised the paper, and provided funding support. All authors contributed to the paper and approved the submitted version.

COMPETING INTERESTS

The authors declare no competing interests.

ADDITIONAL INFORMATION

Supplementary information The online version contains supplementary material available at <https://doi.org/10.1038/s41612-023-00381-8>.

Correspondence and requests for materials should be addressed to Anmin Duan.

Reprints and permission information is available at <http://www.nature.com/reprints>

Publisher's note Springer Nature remains neutral with regard to jurisdictional claims in published maps and institutional affiliations.



Open Access This article is licensed under a Creative Commons Attribution 4.0 International License, which permits use, sharing, adaptation, distribution and reproduction in any medium or format, as long as you give appropriate credit to the original author(s) and the source, provide a link to the Creative Commons license, and indicate if changes were made. The images or other third party material in this article are included in the article's Creative Commons license, unless indicated otherwise in a credit line to the material. If material is not included in the article's Creative Commons license and your intended use is not permitted by statutory regulation or exceeds the permitted use, you will need to obtain permission directly from the copyright holder. To view a copy of this license, visit <http://creativecommons.org/licenses/by/4.0/>.

© The Author(s) 2023